Astronomy
&
Astrophysics

New abundances of planetary nebulae in the Galactic Bulge[*],[**]

A. V. Escudero, R. D. D. Costa, and W. J. Maciel

Departamento de Astronomia, IAG/USP, C.P. 3386, 01060-970 São Paulo – SP, Brasil
e-mail: escudero@astro.iag.usp.br; maciel@astro.iag.usp.br

Abstract. New observations and derived chemical abundances are reported for a sample of 57 bulge planetary nebulae (PN). Together with our previous results, a total of over a hundred objects have been analyzed, which constitute one of the largest samples of bulge nebulae studied under homogeneous conditions, including equipment and reduction procedures. In general, our data show a good agreement with some recent results in the literature, in the sense that the average abundances of bulge PN are similar to those from disk objects, however showing a larger dispersion.

Key words. planetary nebulae: general – galaxies: bulges – techniques: spectroscopic

1. Introduction

In the past few years, many papers have been published dealing with the kinematics and abundances of the galactic bulge. Most of these works on bulge abundances are concerned with heavy elements produced by supernovae, so that light elements such as helium and nitrogen have had a smaller share of attention.

Planetary nebulae (PN) constitute an important tool in the study of the chemical evolution of the bulge, providing accurate determinations of the abundances of light elements produced by progenitor stars of different masses. In fact, PN offer the possibility of studying both light elements produced in low mass stars, such as He and N, and also heavier elements which result from the nucleosynthesis of large mass stars, such as oxygen, sulfur and neon, which are present in the interstellar medium at the stellar progenitor formation epoch.

Previous determinations of chemical abundances of bulge PN have shown that, on average, these objects have abundances similar to disk planetary nebulae (Escudero & Costa 2001; Liu et al. 2001; Cuisinier et al. 2000; Costa & Maciel 1999; Ratag et al. 1997). However, the total number of bulge PN with accurate abundances is still small; furthermore, a correlation between the chemical abundances and bulge kinematics is still to be determined, in contrast with the observed properties of the galactic disk.

In the present paper, we report new observations and derive chemical abundances for a sample of 57 bulge PN. These results are compared with previous data from our own group

and other groups as well, both regarding the galactic bulge and other galactic systems, such as the galactic disk and halo.

In Sect. 2 we present our new observations for a sample of bulge PN and comment on the reduction procedure. In Sect. 3 we present our method to derive the chemical abundances. A discussion of the main uncertainties of the physical parameters is given in Sect. 4. A comparison of our results with published data is given in Sect. 5, and in Sect. 6 we discuss our results an present our main conclusions.

2. Observations and data reduction

2.1. Observations

In this work we present results for 57 new PNe, extending and completing a previous paper (Escudero & Costa 2001), in which we have presented our results for a sample of 45 objects toward the galactic bulge.

The objects were selected according to their distances, taken from the literature (Schneider & Buckley 1996; van de Steene & Zijlstra 1995; Zhang 1995), adopting as probable bulge objects those with heliocentric distances greater than 5 kpc. In spite of the sometimes larger uncertainties for these distances, this is still the best homogeneous criterion to define the sample. Other criteria like diameters, Hβ or radio fluxes are even less reliable. It should be noted that in this paper we did not use the same criterion used by Escudero & Costa (2001), where all objects towards the bulge from Beaulieu et al. (1999) and Kohoutek (1994) were observed. These objects do not have distance determinations, but as most of them have diameters smaller than 20″, they should be at or near the bulge according to the criteria of Gathier et al. (1983).

Adopted distances are listed in Table 3. We divided our sample in two samples: those with heliocentric distances
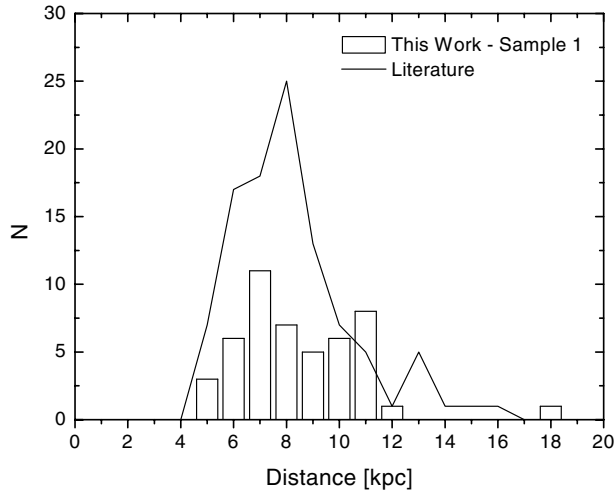
Fig. 1. Distance distribution for our sample 1 (objects with heliocentric distances greater than 5 kpc) and objects from the literature.

greater than 5 kpc (sample 1), and those with heliocentric distancies smaller than 5 kpc or unknown (sample 2). Figure 1 displays the distance distribution for our sample 1 objects, combined with objects chosen from the literature (see Sect. 5 for detailed references). Adopting these distances and the criteria mentioned above we would expect some 80% of the sample to be in the galactic bulge, a fraction similar to the estimates given by Pottasch (1990), to which the reader is refered for a detailed discussion on the characterization of galactic bulge PN.

The program objects were observed with two telescopes: 1.60 m LNA (Laboratório Nacional de Astrofísica, Brasópolis – Brasil), and 1.52 m ESO (European Southern Observatory). Each object was observed at least twice in order to secure good final spectra. We selected the exposure time for each object in order to have a good S/N in the region of the Hγ line, due to the importance of the [OIII]λ4363 line in the temperature diagnostics.

For all objects, we used the long slit of 2 arcsecs width. At LNA we used a 300 l/mm grid with 4.4 A/pix dispersion, and at ESO the used grid was 600 l/mm with 2.4 A/pix dispersion. Each night at least three spectrophotometric standard stars were observed to improve the flux calibration.

Table 1 list the PN G designation (first column), the usual names of the observed objects (Col. 2), equatorial coordinates for epoch 2000 (Cols. 3 and 4), date of observation (Col. 5), observatory (Col. 6) and the exposure time in seconds (last column). For some objects, spectra were taken with different exposure times: a short exposure to measure the Balmer series lines (and therefore to derive interstellar extinction), and a longer exposure (usually with Hα saturated) to measure the fluxes of lower intensity lines.

Table 2 (available electronically) display the line fluxes of the reddened lines. For the cases where the line blend [OII]$\lambda\lambda$7319, 7330 was impossible do separate, their intensities are added in the [OII]λ7319 column.

Figure 2 shows typical spectra from our sample. The upper panel shows M 3-26, an object with well defined lines,

and the other shows KFL 4, a poorer object, observed with lower resolution.

2.2. Interstellar extinction

The application of the extinction curve of Fitzpatrick (1999) had better results than the use of the curve of Cardelli et al. (1989) (CCM), when we compared the predicted Hγ/Hβ = 0.47, (adopting Osterbrock's case B) with the calculated values after interstellar extinction correction. A small difference between the two curves in the Hγ and Hα regions (see Fig. 6 of Fitzpatrick 1999) results in a significant discrepancy with respect to the recombination values when we use the CCM curve. Using the Fitzpatrick (1999) curve this difference is considerably reduced. These results are displayed in Fig. 3, where both distributions are plotted. Is easy to see that the distribution of Hγ/Hβ ratios calculated with the Fitzpatrick curve is narrower and that its center is closer to the theoretical value of 0.47.

In order to bring the value of Hγ closer to the recombination value using the CCM curve, it would be necessary to use a value of the ratio of total to selective absorption R_V higher than 6.0, which is extremely large and inconsistent with the value determined by Stasińska et al. (1992). The main consequence for the poor interstellar correction in the Hγ region is the poor determination of the electron temperature for O^{++}. High O[III]λ4363 values would result in overestimated temperatures and low abundance values, as shown by other authors (Köppen et al. 1991; Stasińska et al. 1998) who expected that some of the objects lacking O[III]λ4363 might be the most metal rich.

In this work we have used the Fitzpatrick (1999) extinction curve, deriving $E(B-V)$ from the observed Balmer ratio Hα/Hβ and adopting the theoretical value Hα/Hβ = 2.85, with R_V = 3.1.

Figure 4 displays the distribution of $E(B - V)$ derived for sample 1 (see Sect. 2.1) compared with data from the literature and from Escudero & Costa (2001). It can be seen that the distribution for the present data agrees well with our previous work, and is in reasonable agreement with data from the literature, which are on average nearer the galactic center.

3. Determination of chemical abundances

3.1. Physical parameters

The quality of the physical parameters is crucial for a good derivation of chemical abundances, as line emissivities of the ions are extremely sensitive to the electron temperature and density of the nebulae.

For the determination of electron temperatures we used the following line ratios for oxygen and nitrogen: [OIII]$\lambda\lambda$4363, 5007 and [NII]$\lambda\lambda$5755, 6584, from which we can obtain estimates of the electron temperature for high and low ionization regions. The electron density was derived from the sulfur line ratio [SII]$\lambda\lambda$6716, 6731, giving therefore an average value for the whole nebula. Excitation classes were also defined for the object following the Webster (1988) criterium. For each nebula

Table 1. Log of the observations.

PN G	Name	RA(2000)	Dec (2000)	Date of Obs.	Place	Exp. Time (s)
000.4-02.9	M 3-19	17 58 18	−30 00 10	19-May-01	ESO	2 × 900
000.4-01.9	M 2-20	17 54 25	−29 36 09	19-May-01	ESO	1 × 600
000.7+04.7	H 2-11	17 29 26	−25 49 06	11-Jun.-02	LNA	2 × 1800
000.9-02.0	Bl 3-13	17 56 02	−29 11 15	22-May/11-Jul.-01	ESO	2 × 900, 2 × 2400
001.2+02.1	He 2-262	17 40 15	−26 43 21	19-May-01	ESO	2 × 1200
001.7+05.7	H 1-14	17 28 02	−24 25 28	12-Jul.-01	ESO	2 × 1800
002.0-02.0	H 1-45	17 58 23	−28 14 54	19-May-01	ESO	3 × 600
002.2-06.3	H 1-63	18 16 19	−30 07 36	13-Jul.-01	ESO	2 × 1200
002.2-02.5	KFL 2	18 01 00	−28 16 19	22-May-01	ESO	2 × 1800
002.6+08.2	H 1-11	17 21 18	−22 18 36	14-Jul.-01	ESO	2 × 1200
003.0-02.6	KFL 4	18 02 52	−27 41 02	22-May/15-Jul.-01	ESO	2 × 1200, 1 × 3600, 1 × 1800
003.3-07.5	KFL 19	18 23 09	−29 43 25	12-Jul.-01	ESO	2 × 1800
003.6-02.3	M 2-26	18 03 12	−26 58 31	22-May-01	ESO	2 × 1200
004.0-05.8	Pe 1-12	18 17 43	−28 17 24	13-Jul.-01	ESO	1 × 1200, 1 × 1800
004.8-05.0	M 3-26	18 16 09	−27 14 50	12-Jul.-01	ESO	2 × 900
004.8+02.0	H 2-25	17 49 02	−23 42 57	19/21-May-01	ESO	1 × 900, 1 × 1200
005.5+02.7	H 1-34	17 48 08	−22 46 48	21-May-01	ESO	2 × 1200
005.7-05.3	M 2-38	18 19 26	−26 35 20	13-Jul.-01	ESO	2 × 120
006.4+02.0	M 1-31	17 52 41	−22 21 57	19-May-01	ESO	1 × 600, 2 × 300
006.8+02.3	Th 4-7	17 52 21	−21 51 12	19-May-01	ESO	2 × 900
007.0-06.8	Vy 2-1	18 27 59	−26 06 48	13-Jun.-01	LNA	2 × 300
008.1-04.7	M 2-39	18 22 02	−24 10 41	11-Jun.-02	LNA	2 × 300
008.2+06.8	He 2-260	17 38 57	−18 17 35	12-Jul.-01	ESO	1 × 1200, 1 × 600
008.8+05.2	Th 4-2	17 46 09	−18 39 33	12-Jul.-01	ESO	2 × 1800
009.4-09.8	M 3-32	18 44 43	−25 21 34	12-Jul.-01	ESO	2 × 900
009.6-10.6	M 3-33	18 48 13	−25 28 56	13-Jul.-01	ESO	2 × 600
009.8-04.6	H 1-67	18 25 06	−22 34 51	11-Jun.-02	LNA	2 × 900
010.7-06.7	Pe 1-13	18 34 53	−22 43 18	13-Jun.-01	LNA	1 × 600, 2 × 1200
011.0+06.2	M 2-15	17 46 54	−16 17 27	12-Jul.-01	ESO	2 × 900
011.1+11.5	M 2-13	17 28 34	−13 26 17	13-Jul.-01	ESO	2 × 1200
011.3-09.4	H 2-48	18 46 35	−23 26 41	10-Jun.-02	LNA	2 × 30, 2 × 300
013.4-03.9	M 1-48	18 29 30	−19 06 51	10-Jun.-02	LNA	2 × 1200
013.7-10.6	Y-C 2-32	18 55 31	−21 49 39	13-Jul.-01	ESO	2 × 600
018.6-02.2	M 3-54	18 33 04	−13 44 21	11-Jun.-02	LNA	2 × 1200
018.9+03.6	M 4-8	18 12 06	−10 43 05	11-Jun.-02	LNA	2 × 1800
018.9+04.1	M 3-52	18 10 30	−10 28 60	11-Jun.-02	LNA	2 × 1800
352.0-04.6	H 1-30	17 45 08	−38 08 55	10-Jun.-02	LNA	2 × 1200
352.1+05.1	M 2-8	17 05 31	−32 32 08	13-Jun.-01	LNA	2 × 800
352.8-00.2	H 1-13	17 28 28	−35 07 32	22-May-01	ESO	2 × 1200
353.7+06.3	M 2-7	17 05 13	−30 32 14	11-Jul.-01	ESO	2 × 900
353.8-01.2	K 6-3	17 35 27	−34 47 42	14-Jul.-01	ESO	1 × 2400, 1 × 3600
354.6-01.7	K 6-5	17 38 54	−34 27 39	15-Jul.-01	ESO	2 × 3600
356.1+02.7	Th 3-13	17 25 19	−30 40 44	20-May-01	ESO	2 × 1200
356.3-00.3	Th 3-34	17 37 45	−32 15 29	14-Jul.-01	ESO	1 × 3600, 1 × 2400
356.7-06.4	H 1-51	18 04 30	−34 58 00	15-Jul.-01	ESO	2 × 1800
356.7-04.8	H 1-41	17 57 19	−34 09 50	10-Jun.-02	LNA	2 × 1200
357.0+02.4	M 4-4	17 28 50	−30 07 46	21-May-01	LNA	2 × 1200
357.1-04.7	H 1-43	17 58 15	−33 47 39	11-Jun.-02	LNA	2 × 300, 2 × 1200
357.2-04.5	H 1-42	17 57 25	−33 35 44	11-Jun.-02	LNA	2 × 150
358.3-02.5	Al 2-O	17 51 45	−32 03 04	22-May-01	ESO	2 × 1800
358.5-04.2	H 1-46	17 59 02	−32 21 44	11-Jun.-02	LNA	2 × 150, 1 × 600
358.5-02.5	M 4-7	17 51 45	−31 36 00	22-May-01	ESO	2 × 1800
358.6+01.8	M 4-6	17 35 14	−29 03 11	13-Jul.-01	ESO	2 × 1800
358.8+04.0	Th 3-15	17 27 09	−27 44 20	11-Jun.-02	LNA	2 × 1800
359.8+05.6	M 2-12	17 24 01	−25 59 23	11-Jul.-01	ESO	2 × 900
359.8+06.9	M 3-37	17 19 13	−25 17 15	12-Jul.-01	ESO	2 × 1800
359.9+05.1	M 3-9	17 25 43	−26 11 54	13-Jul.-01	ESO	2 × 1800

Table 2. Line fluxes (available electronically).

Line	Al 2-0	Bl 3-13	H1-11	H1-13	H1-14	H1-30	H1-34	H1-41	H1-42	...
[OII]λ3726+29	179.3	–	7.4	–	48.0	83.1	57.7	31.7	18.5	...
[NeIII]λ3869	124.5	49.3	76.6	74.8	100.8	112.9	–	59.4	88.5	...
:										
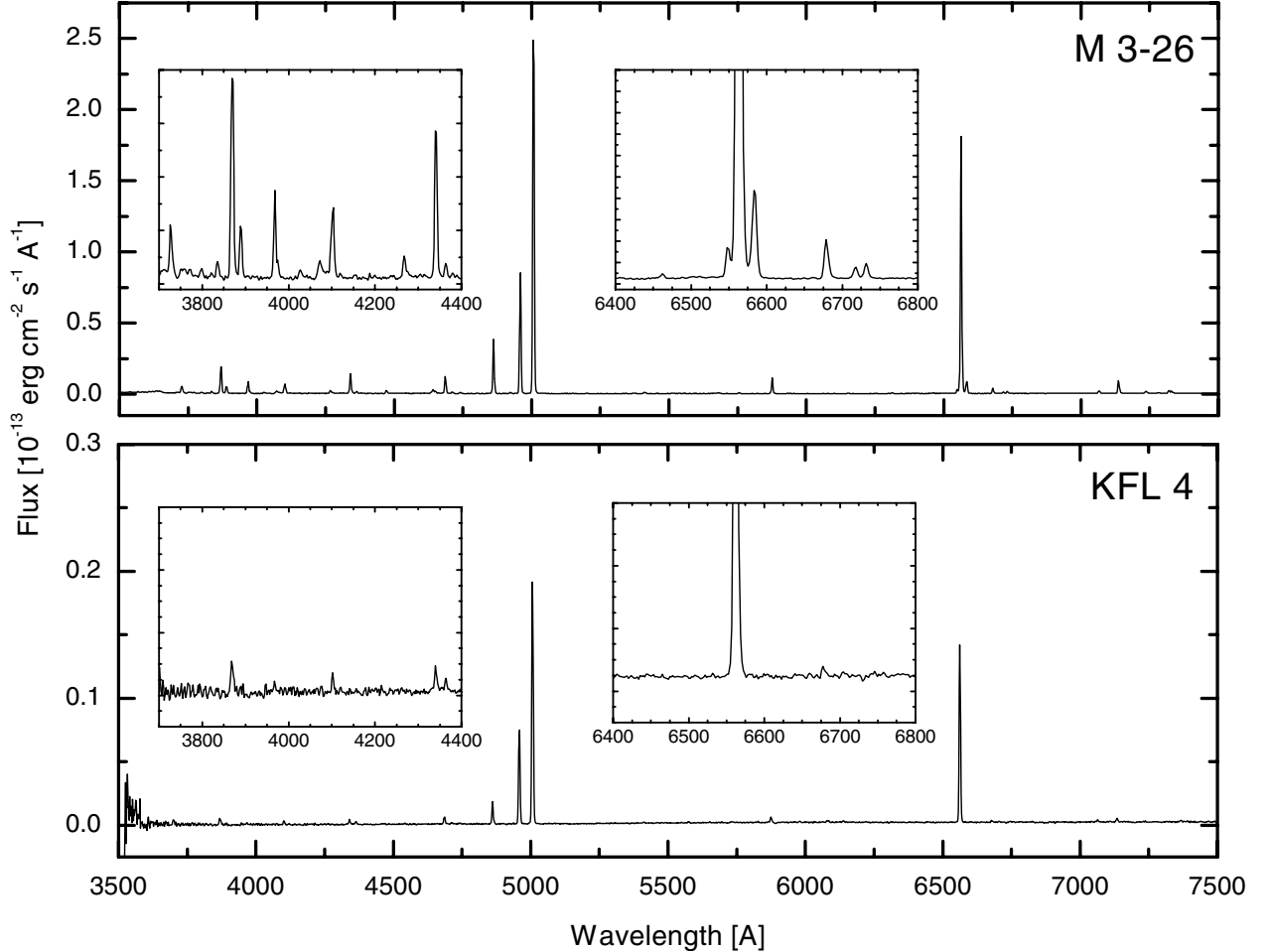
Fig. 2. Typical spectra from our sample. The upper panel shows M 3-26, with well defined lines, and the lower panel shows KFL 4, a poorer object.

the Hβ surface flux was calculated using the derived Hβ flux and the fraction of the nebula within the slit.

In Table 3 we give the observed (Col. 2) Hβ intensities and corrected by interstellar extinction (in erg cm^{-2} s^{-1}) (Col. 3), diameters in arcsecs from Acker et al. (1992) (Col. 4), Hβ surface flux (in erg cm^{-2} s^{-1} arcsec^{-2}), the interstellar extinction $E(B-V)$ (Col. 6), the electron density in 10^3 cm^{-3} (Col. 7), the electron temperatures in 10^4 K (Cols. 8 and 9), excitation class (Col. 10) and heliocentric distances in kpc (Col. 11).

3.2. Ionic abundances

In order to calculate abundances for the ions N$^+$, O^0, O$^+$, O^{++}, S$^+$, S^{++}, Ar^{++}, Ne^{++}, we have used the fits by Alexander & Balick (1997) that show a good agreement with ionic abundances obtained from statistical balance equations. For the helium ions (He$^+$, He^{++}) we used the recombination coefficients

from Péquignot et al. (1991), with the coefficients for He$^+$ collisional excitation correction derived by Kingdon & Ferland (1995). Only for Cl^{++}, not present in the Alexander & Balick (1997) tables, we used the statistical balance equation for the [ClIII]$\lambda\lambda$5518+5538 lines.

In particular, the O$^+$ abundance can be derived from two pairs of lines: λ3727+29 and λ7319+30. There is however a systematic difference between the resulting values, with some tendency to higher abundances for the red pair. These differences are shown in Fig. 2. In this figure, the dashed line is a linear fit for our sample. To explain this difference, observed also by other authors, we raised four alternatives: interstellar extinction, data reduction, electron temperature and density variations, and O^{++} recombination.

- Interstellar Extinction: one of the factors that could cause this difference is a poor interstellar extinction correction. To check this, we corrected all spectra with two interstellar

Table 3. Physical parameters and distances.

| PNe	$\log_{10}(H\beta)$	$\log_{10}(H\beta)_0$	Diam	$\log_{10}(SF)$	$E(B-V)$	n[SII]	T[NII]	T[OIII]	EC	Dist
Al 2-O	−14.27	−12.47	–	–	1.22	0.40	0.86	1.53	9	5.69
Bl 3-13	−13.41	−11.69	5.2	−12.71	1.17	1.88	–	0.81	3	6.87
H 1-11	−12.88	−11.55	6.4	−12.66	0.90	1.92	–	0.93	5	6.85
H 1-14	−13.42	−11.70	6.6	−12.82	1.17	0.97	1.51	1.56	6	5.59
H 1-30	−13.10	−11.83	5.4	−12.86	0.86	6.90	0.88	1.01	6	5.21
H 1-34	−13.33	−11.55	–	–	1.20	3.55	0.72	0.9	0.5	10.45
H 1-41	−12.36	−11.88	9.6	−13.16	0.33	3.51	1.11	0.96	6	5.98
H 1-43	−12.43	−11.46	2.0	−12.06	0.66	9.52	0.55	–	0	11.13
H 1-45	−13.22	−11.11	6.0	−12.19	1.43	–	–	4.47	7	7.65
H 1-46	−12.12	−10.87	–	–	0.85	5.31	1.47	0.96	2	7.29
H 1-63	−11.77	−11.20	7.0	−12.35	0.38	20.00	2.11	1.09	1	11.00
H 1-67	−12.64	−11.83	5.6	−12.88	0.55	1.46	0.99	1.06	7	7.13
H 2-11	−13.91	−11.02	2.7	−11.75	1.96	20.00	0.85	1.02	1	7.90
H 2-25	−13.66	−11.46	4.4	−12.41	1.49	0.52	0.84	–	0.5	11.40
H 2-48	−11.44	−10.54	2.0	−11.14	0.61	13.23	1.32	1.03	0.5	5.49
He 2-260	−12.39	−11.69	10.0	−12.99	0.47	20.00	1.07	–	0.5	11.72
He 2-262	−13.84	−11.43	4.0	−12.33	1.63	4.19	–	–	4	6.66
KFL 2	−14.12	−13.40	5.4	−14.43	0.49	–	–	1.70	9	11.07
KFL 4	−14.00	−12.75	3.0	−13.53	0.85	–	–	1.38	7	17.66
KFL 19	−13.49	−13.28	7.8	−14.48	0.14	–	–	0.89	3	11.38
M 1-48	−12.66	−11.79	4.8	−12.77	0.59	1.58	0.84	0.87	5	9.46
M 2-7	−12.84	−11.86	7.8	−13.05	0.66	0.83	0.75	–	1	7.32
M 2-8	−12.37	−11.29	4.2	−12.21	0.73	1.67	0.95	1.05	7	7.15
M 2-12	−12.52	−11.46	5.0	−12.46	0.71	8.24	0.71	0.71	0	8.15
M 2-13	−12.73	−11.77	7.0	−12.91	0.66	4.65	1.00	0.91	>4	10.26
M 2-15	−12.65	−11.61	5.8	−12.68	0.70	2.28	1.47	0.94	6	6.66
M 2-20	−12.93	−11.16	6.6	−12.29	1.19	1.09	0.79	0.88	5	6.08
M 2-26	−13.28	−11.94	9.2	−13.20	0.91	0.31	0.81	0.99	2	8.20
M 2-38	−13.06	−12.97	9.3	−14.24	0.07	0.89	1.57	1.21	9	7.54
M 2-39	−12.19	−11.21	3.2	−12.02	0.66	2.92	1.11	3.35	3−4	10.05
M 3-19	−13.65	−12.99	5.7	−14.05	0.45	–	–	1.24	3−5	8.32
M 3-26	−12.63	−12.05	8.6	−13.28	0.40	1.18	2.47	1.01	7	7.44
M 3-32	−12.26	−11.69	6.0	−12.77	0.39	1.93	1.28	0.93	5	6.90
M 3-33	−12.37	−11.94	5.0	−12.94	0.29	1.25	–	1.07	6	8.52
M 3-37	−13.84	−12.16	10.0	−13.46	1.14	0.85	0.94	0.99	5	9.97
M 3-52	−14.40	−12.39	11.6	−13.76	1.36	0.35	0.9	–	5	10.70
M 3-54	−13.24	−11.86	–	–	0.93	1.40	–	1.09	7	8.87
M 4-4	−14.09	−11.63	6.6	−12.75	1.66	0.96	0.9	–	7	8.33
M 4-6	−14.03	−11.00	–	–	2.05	5.81	1.29	1.07	5	6.53
M 4-7	−14.18	−11.68	–	–	1.69	1.58	1.29	1.41	5	5.08
M 4-8	−13.47	−11.22	–	–	1.52	7.33	1.05	–	0.5	9.32
Pe 1-12	−13.30	−12.98	9.6	−14.26	0.22	9.58	1.35	1.35	–	8.82
Pe 1-13	−12.96	−12.32	7.6	−13.50	0.43	–	–	1.58	9	11.42
Th 3-13	−14.10	−10.95	–	–	2.14	2.52	2.22	–	2	10.31
Th 3-15	−13.75	−12.04	–	–	1.16	0.60	–	1.2	2	10.16
Th 4-2	−13.57	−12.81	19.0	−14.39	0.52	0.39	0.85	1.02	7	11.29
Th 4-7	−13.88	−12.40	6.0	−13.48	1.00	2.11	1.16	1.43	>4	5.56
Vy 2-1	−12.03	−12.03	7.0	−13.11	0.00	0.84	0.94	0.73	3	5.58
H 1-13	−13.62	−10.34	9.6	−11.62	2.22	3.73	1.08	0.83	5	1.43
H 1-42	−11.82	−10.96	5.8	−12.03	0.58	2.41	1.28	0.96	4	4.85
H 1-51	−13.83	−12.87	13.2	−14.30	0.65	0.24	0.79	1.57	5	–
K 6-3	−14.65	−11.31	–	–	2.26	1.76	0.75	1.31	1	–
K 6-5	−15.13	−11.53	–	–	2.44	1.15	1.00	–	–	–
M 1-31	−12.63	−10.86	–	–	1.20	3.96	1.11	0.75	3	4.50
M 3-9	−13.43	−11.74	17.0	−13.27	1.15	1.96	–	1.03	6	3.57
Th 3-34	−15.18	−11.04	–	–	2.81	5.29	2.53	2.03	9	–
YC 2-32	−12.33	−11.98	15.0	−13.45	0.24	3.89	–	0.94	5	–
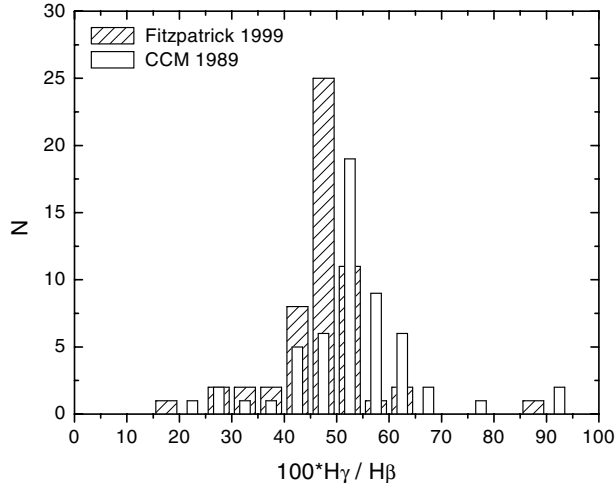
Fig. 3. The distribution of the Hγ/Hβ values corrected by the Fitzpatrick (1999) (hatched) and Cardelli et al. (1989) (white) interstellar extinction curves.
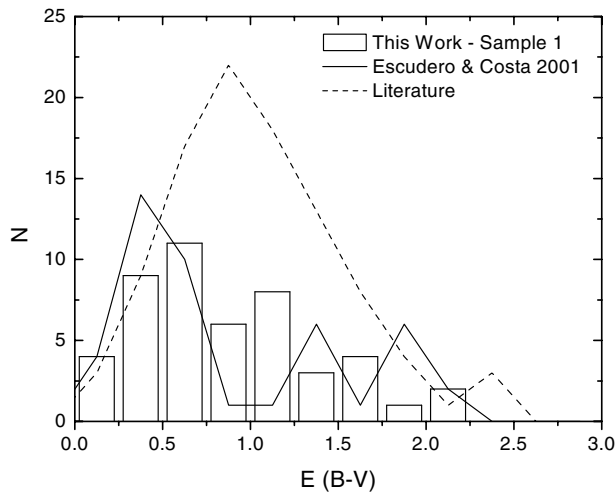

Fig. 4. Distribution of $E(B-V)$ values for our sample. Also included are the distribution of Escudero & Costa (2001) and data from the literature.

extinction laws (Fitzpatrick 1999 and CCM 1989) using two extreme values for R_V: 2.1 e 5.9. The results do not imply a significant variation of the O^{++} abundance in any case. The only possibility to invoke extinction to explain such a difference would be a new, totally distinct interstellar extinction law, which seems unrealistic, since most of the extinction comes from the disk

- Data reduction: as the two line pairs are in opposite regions of the spectrum, poor flux calibration could affect the final data. However, it is unlikely that this effect could affect all data. Furthermore, this effect appears also in other, independent works (Stasińska et al. 1998).

- Temperature and density variations: this can be an important factor in abundance calculations (Viegas & Clegg 1994). Regions with high density in the inner part of a planetary nebula contribute to the intensity of $\lambda7319+30$, but not to $\lambda3727$ (Mathis et al. 1998). With respect to the density, as the intensity of the [SII] line relative to Hβ depends on the density (Alexander & Balick 1997), this value will represent
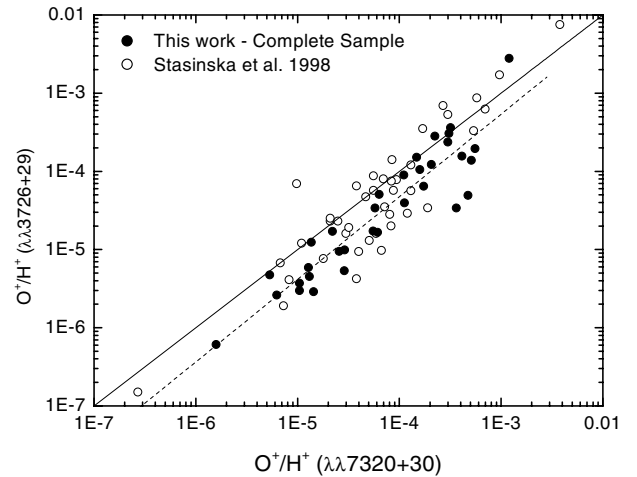

Fig. 5. A comparison of the O$^+$ ionic abundance from the blue (3727+29) and red (7319+30) lines, respectively.

preferentially lower density regions, and this effect would be more evident for bulge objects due to their smaller angular sizes. For disk objects, the slit would cover only the central part of a planetary nebula and the effect is not as important as for bulge nebulae.

- Recombination of O^{++}: For nebulae with low density and electron temperature, dielectronic recombination of O^{++} may play an important role (Rubin 1986; Aller & Keyes 1987), leading to differences in the derived ionic abundances.

Figure 5 displays a comparison between the O$^+$ ionic abundance derived from the blue (3726+29) and the red (7320+30) lines, both for our sample and that from Stasinska et al. (1998). In the figure, the continuous line is a $y = x$ plot and the dashed line is a linear fit for all the points. As can be seen, there is a small discrepancy between both determinations, with a tendency for higher abundances when the red lines are used. The same effect appears for both samples. As the final explanation is still an open issue, we adopted the blue pair to derive the O$^+$ abundance like most of the other works in the literature:

$$\log (O^+_{3727}/H^+) = (-0.1 \pm 0.3) + (1.06 \pm 0.08) \log (O^+_{7325}/H^+).$$

The derivation of sulfur abundance requires both S$^+$ and S^{++} ions. For those objects where S^{++} was not available we adopted the same technique used by Kingsburgh & Barlow (1994), deriving the S^{++} abundance from the relation between ratios S^{++}/S$^+$ and O^{++}/O$^+$. This relation was derived from our data, as can be seen in Fig. 6. In the figure, filled and open circles represent the points included in the fit, and crosses are abundances poorly determined, which were not included. The dotted line is a $y = x$ relation and the continuous line is the best fit represented by the relation:

$$\log (S^{++}/S^+) = (0.21 \pm 0.08) + (0.73 \pm 0.06) \log (O^{++}/O^+).$$

3.3. Elemental abundances

The final abundances are listed in Table 4. The objects separated by an horizontal line in the final of Table 4 and also in
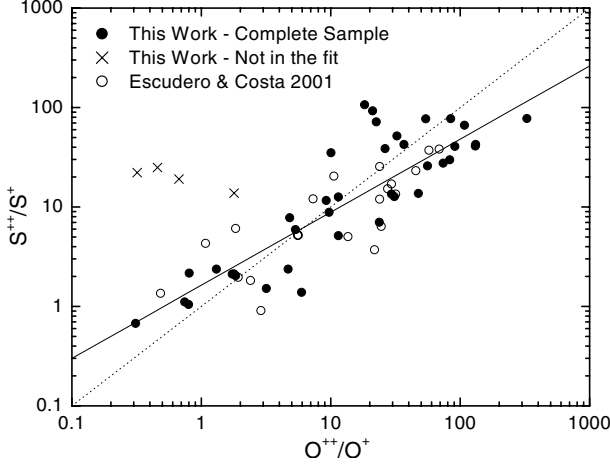
Fig. 6. Relation between S^{++}/S^+ and O^{++}/O^+.

Table 3 are those from our sample 2 (see Sect. 2.1). In the discussion on the abundance distribution (see Sect. 5) we do not include these objects.

Since it is not possible to get the chemical abundances of all ions of a given element, we use the ICF method (Ionization Corrections Factors) to derive the elemental abundances, as in our previous works. For details, see Escudero & Costa (2001), Costa et al. (1996) and references therein.

The adopted ICF for oxygen and nitrogen are those suggested by Peimbert & Torres-Peimbert (1977); for sulfur and neon we used the ICF provided by Kingsburgh & Barlow (1994), except for those objects for which S^{++} is not available; in this case we adopted the value derived by the relation given in the last section. For argon we used the ICF provided by Freitas Pacheco et al. (1993). These ICFs are listed below.

$$\frac{He}{H} = \frac{He^+}{H^+} + \frac{He^{++}}{H^+}$$

$$\frac{O}{H} = \left(\frac{O^{++}}{H^+} + \frac{O^+}{H^+}\right)\frac{He}{He^+}$$

$$\frac{N}{H} = \frac{N^+}{H^+}\frac{O}{O^+}$$

$$\frac{S}{H} = \left(\frac{S^+}{H^+} + \frac{S^{++}}{H^+}\right)\left(1 - \left(1 - \frac{O^+}{O}\right)^3\right)^{-1/3}$$

$$\frac{Ar}{H} = 1.34\frac{Ar^{++}}{H^+}\frac{O}{O^{++}}$$

$$\frac{Ne}{H} = \frac{Ne^{++}}{H^+}\frac{O}{O^{++}}.$$

4. Errors in the physical parameters and chemical abundances

In Escudero & Costa (2001) typical errors were derived through a Monte Carlo simulation, based on the line intensities

Table 4. Chemical abundances.

Name	He	$\epsilon(N)$	$\epsilon(O)$	$\epsilon(S)$	$\epsilon(Ar)$	$\epsilon(Ne)$
Al 2-O	0.160	8.43	8.66	6.57	6.78	7.95
Bl 3-13	0.105	7.68	8.91	7.14	6.54	8.06
H 1-11	0.106	8.02	8.67	6.87	6.28	7.95
H 1-14	0.103	7.62	8.27	6.39	5.66	7.38
H 1-30	0.147	8.78	8.76	6.66	6.86	8.13
H 1-34	0.013	8.14	8.45	7.04	6.34	–
H 1-41	0.123	7.95	8.64	6.81	6.22	7.85
H 1-43	0.011	8.44	8.84	6.80	–	–
H 1-45	0.099	7.39	7.52	5.69	4.97	6.84
H 1-46	0.096	7.93	8.35	6.95	6.16	7.40
H 1-63	0.059	7.48	8.06	6.86	6.09	6.97
H 1-67	0.125	8.50	8.75	7.09	6.64	8.00
H 2-11	0.151	8.16	8.29	6.56	6.64	–
H 2-25	0.081	7.56	8.26	6.74	6.70	–
H 2-48	0.048	7.12	7.93	6.41	6.03	–
He 2-260	0.009	7.14	8.18	6.29	6.97	–
He 2-262	0.118	7.82	8.48	6.66	6.24	7.55
KFL 2	0.113	–	8.24	–	5.99	7.33
KFL 4	0.099	–	8.34	–	5.71	7.28
KFL 19	0.080	7.38	8.65	6.93	6.06	7.64
M 1-48	0.143	8.65	8.84	7.09	6.88	8.33
M 2-7	0.137	7.91	8.74	6.61	6.80	7.91
M 2-8	0.223	8.50	8.54	6.04	6.40	7.81
M 2-12	0.010	7.96	8.56	6.60	7.86	–
M 2-13	0.117	8.22	8.72	6.96	6.48	8.07
M 2-15	0.128	8.30	8.61	6.95	6.38	8.00
M 2-20	0.081	8.07	8.78	6.83	6.43	–
M 2-26	0.161	8.77	8.49	6.88	6.65	7.53
M 2-38	0.152	8.57	8.58	7.28	6.73	7.78
M 2-39	0.107	6.94	7.48	5.45	5.64	6.76
M 3-19	0.101	7.27	8.00	–	6.29	7.22
M 3-26	0.137	8.43	8.40	6.99	6.36	7.92
M 3-32	0.132	8.27	8.56	6.95	6.35	7.87
M 3-33	0.072	7.72	8.62	6.57	6.00	7.84
M 3-37	0.092	8.34	8.86	6.72	6.74	8.34
M 3-52	0.129	8.58	8.79	7.15	6.91	–
M 3-54	0.122	7.33	8.67	6.52	6.24	7.97
M 4-4	0.154	8.74	8.92	7.25	6.78	–
M 4-6	0.111	8.47	8.71	6.98	6.30	8.01
M 4-7	0.102	7.94	8.33	6.43	5.79	7.59
M 4-8	0.015	7.24	8.03	6.24	6.66	–
Pe 1-12	0.114	7.90	8.63	5.41	6.36	7.82
Pe 1-13	0.099	–	9.03	–	6.66	8.29
Th 3-13	0.089	7.33	7.61	6.10	5.98	–
Th 3-15	0.107	7.62	8.06	6.15	5.89	–
Th 4-2	0.180	8.72	8.50	6.95	6.75	7.79
Th 4-7	0.072	7.70	8.35	6.47	5.90	7.49
Vy 2-1	0.145	9.04	8.94	6.23	6.94	8.10
H 1-13	0.123	8.84	8.99	7.47	6.67	8.20
H 1-42	0.106	8.27	8.69	6.97	6.15	7.94
H 1-51	0.098	8.27	9.51	6.94	7.72	9.38
K 6-3	0.128	7.98	8.33	6.40	6.49	–
K 6-5	0.159	9.12	8.57	7.32	6.88	–
M 1-31	0.161	9.02	8.98	7.69	6.89	8.28
M 3-9	0.059	7.69	8.68	5.19	6.34	8.05
Th 3-34	0.193	9.15	8.14	7.08	6.43	–
Y-C 2-32	0.088	7.59	8.59	6.61	6.19	7.81

and their errors, which requires the same exposure time for all measurements. This is not the case for the present work, so we examined the effect of these uncertainties on the abundances.

From Escudero & Costa (2001), we have estimated average errors to the abundances of 0.023, 0.18, 0.17, 0.24 and 0.19, respectively for He, N, O, S and Ar. However, it should be remembered that errors are highly affected by interstellar extinction, in the sense that objects that have higher extinction should have greater errors in the abundances, on the average, depending also on the exposition time and the size of the telescope. Therefore, abundances of bulge objects, that have high extinction, typically have higher errors than disk objects, so that we can estimate the uncertainties in the abundances of bulge nebulae to be roughly 0.2 dex, apart from He/H.

4.1. Physical parameters

One of the main error sources in the chemical abundances are the uncertainties in electron temperatures and densities, as discussed previously. Low S/N in weaker diagnostic lines, as well as internal variations in the physical parameters certainly affect the final abundances. As discussed in Sect. 3.2, electron densities derived from [SII] can be underestimated since the emissivity of this line depends on density.

4.2. Helium

The main factors that affect the helium abundance are the uncertainties in densities and electron temperatures. Depending on these parameters, the correction due to collisional excitation can reach 50%. Therefore, errors in the physical parameters would considerably affect the chemical abundances. The existence of neutral helium would also have an influence on the derived abundances. This was tested on the basis of the criterion proposed by Torres-Peimbert & Peimbert (1977), according to which objects with log $O^+/O > -0.4$ seem to have a substantial contribution of neutral helium. For this sample, 11 objects fit this criterion, indicating that their derived helium abundance should be taken cautiously.

4.3. Abundances from collisionally excited lines

In addition to observational errors and those resulting from the inhomogeneity of the nebulae, the use of ionization correction factors (ICF) to estimate elemental abundances for the elements with collisionally excited lines will include additional error sources.

For nitrogen, O^+ is used as ICF, and small variations in its abundance will affect the nitrogen abundance. The use of O^+_{3727} or O^+_{7325} ionic abundances will imply differences of 0.0 to 0.7 dex in the nitrogen abundance.

The same effect occurs for sulfur, in whose ICF O^+ is also present. Two observational effects affect the sulfur abundance: the dependence of S^+ emissivity with density, and the weak intensity of the line [SIII]$\lambda6312$, which will result in a poor determination of the S^{++} abundance. Therefore, the present sulfur abundances should be taken cautiously.

For oxygen, argon and neon, whose lines are normally intense in planetary nebulae, the main error sources are the uncertainties in the physical parameters.

5. Data from the literature

To compare our data, we collected objects from 5 recent works in the literature: Stasińska et al. (1998), Cuisinier et al. (2000), Cuisinier et al. (1996), Samland et al. (1992) and Köppen et al. (1991). We use only those objects with distances already determined (Schneider & Buckley 1996; van de Steene & Zijlstra 1995; Zhang 1995), and with heliocentric distances greater than 5 kpc.

In Fig. 7 we show the distribution of chemical abundances of He, N and O from the literature and our data.

The results from the first paper of this series are also shown (solid irregular lines). In order to homogenize the results, we rederived the elemental abundances for those data, using the same ionic abundances but adopting the improvements used here: sulfur ICF from Kingsburgh & Barlow (1994); O^+ abundance derived preferentially from the blue doublet, and S^{++} derived acording the procedure described in Sect. 3.2, when necessary.

These results have been obtained using the same instruments and procedures as in the present paper, so that both samples are expected to present a large degree of homogeneity. This fact can be observed in Fig. 7, as the abundance distributions of both samples are similar. Small differences observed at the low end of the He and N abundances can be attributed to the incompleteness of the samples. It can be seen that our abundances show a good similarity to all other data. The nitrogen abundances, that reflect the progenitor mass, show a little more scattering from our objects than the data from literature. This was expected to occur because our objects are more widely distributed in angular position than the literature objects (see Escudero & Costa 2001).

6. Discussion and conclusions

Our results are in agreement with those from other works (see for example Escudero & Costa 2001; Cuisinier et al. 2000), indicating that bulge PNe have mean abundances similar to those from disk objects, however displaying higher dispersion.

Figure 8 displays the relation between excitation classes and helium abundances (panel (a)) and oxygen abundances (panel (b)). The data distribution in panel (a) shows no correlation between the helium abundances and the excitation class; the only exception is that some objects with very low abundances are preferably associated with the lowest excitation classes, which possibly indicates the presence of neutral helium for these objects. On the other hand, the absence of correlation in panel (b) also indicates that our abundance analysis is unbiased with respect to the excitation of the nebulae.

Figure 9 displays several abundance correlations for our sample which are distance independent, combined with data from Escudero & Costa (2001) and the literature.

Oxygen and nitrogen are two key elements for the diagnostics of PNe. Due to strong lines, oxygen abundances are
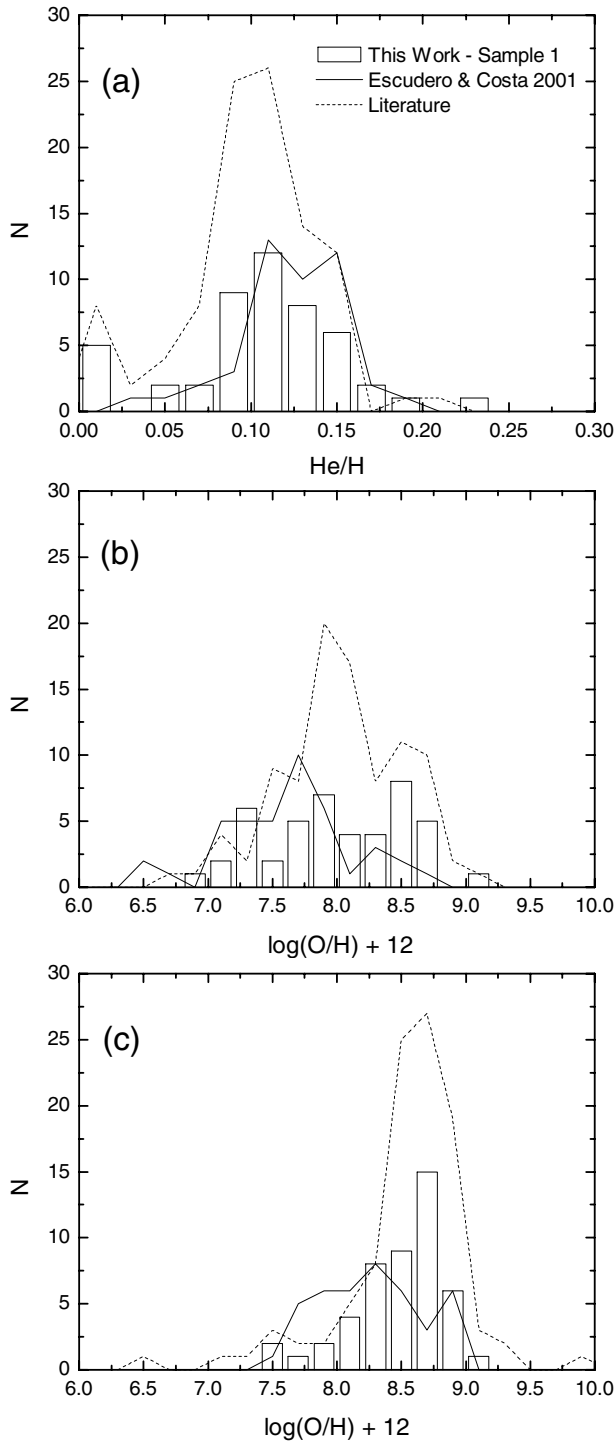
Fig. 7. Distribution of helium, nitrogen and oxygen abundances for this work (sample 1), from Escudero & Costa (2001) and from selected sources in the recent literature (see text).

Fig. 8. Excitation classes versus helium **a)** and oxygen **b)** abundances.

normally very well determined, giving the abundance of the interstellar medium at the progenitor formation epoch. It was already noted that more massive, younger objects like type-I PNe progenitors have oxygen abundance lower than the Sun or type-IIa PNe progenitors (see Costa et al. 1996). The same effect appears in stellar evolution yields (van den Hoek & Groenewegen 1997; Marigo 2001), however for the majority of the lower mass stars, oxygen remains unchanged and can be used to trace the chemical evolution of the interstellar medium.

Nitrogen, on the other hand, has two possible origins: it reflects the abundance of the interstellar medium at the progenitor formation epoch, combined with the material produced by nucleosynthesis during the evolution of the PN progenitor star. Typical yields as a function of the stellar mass are given by van den Hoek & Groenewegen (1997) and Marigo (2001).

Examining the O vs. N diagram displayed in Fig. 9a, a positive correlation between O/H and N/H can be observed. As for the correlation between log (N/O) and O/H (Fig. 9b), this is less evident. We can see that objects with high N/O can have higher or lower oxygen abundances. Those with higher oxygen abundances are similar to the disk type-I PNe, while those with lower abundances are similar to halo objects. On the other hand, objects with low N/O are usually oxygen-rich, which is consistent with the correlation shown in Fig. 9a. Some of these objects may be type-III PNe in the inner disk (see also Maciel 1999) and with the abundances of metal rich bulge giants (Rich 1988). This dispersion in the abundances suggests that the chemical evolution of the bulge cannot be explained in a single formation scenario, so that a composite scenario is required instead.

Another important diagram for the diagnostics of PNe abundances is He × log (N/O), which reflects the chemical enrichment during the stellar evolution of the progenitor. From Fig. 9c it can be seen that there is a reasonably well defined
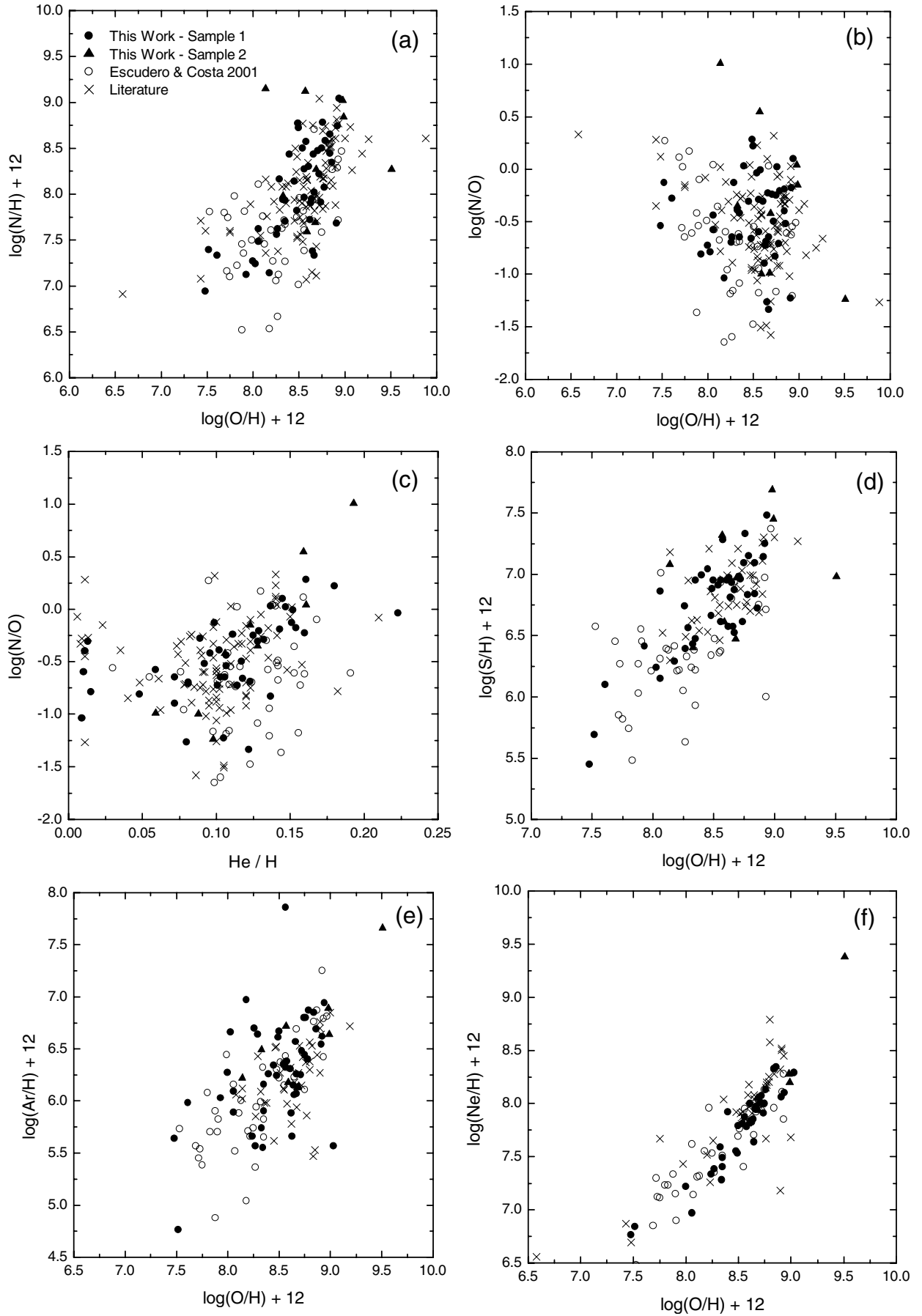
Fig. 9. Abundance correlations from our results and the literature (see Sect. 6).

correlation between He/H and log (N/O), in the sense that helium-rich nebulae are are usually also nitrogen rich, which probably reflects an increasing progenitor mass. A small group of objects apparently have very low He abundances, while their N abundances are normal. This can be explained either by the fact that their progenitor star had smaller masses, which characterizes them as type IIa nebulae, or their He abundances may have been underestimated owing to the presence of neutral helium.

Figures 9d–f display the correlation between the alpha-elements; as they are produced mainly in type II supernovae their correlation reflects the chemical evolution of the interstellar medium from which the progenitor stars are formed. From these figures one can see that lower oxygen abundances imply also lower sulfur, argon and neon abundances.

References

Acker, A., Marcout, J., Ochsenbein, F., Stenholm, B., & Tylenda, R. 1992, ESO-Strasbourg catalogue of galactic planetary nebulae (Garching: ESO)

Alexander, J., & Balick, B. 1997, AJ, 114, 713

Aller, L. H., & Keyes, C. D. 1987, ApJS, 65, 405

Beaulieu, S. F., Dopita, M. A., & Freeman, K. C. 1999, ApJ, 515, 610

Cardelli, J. A., Clayton, G. C., & Mathis, J. S. 1989, ApJ, 345, 245 (CCM)

Costa, R. D. D., de Freitas Pacheco, J. A., & de França Jr., J. A. 1996, A&A, 313, 924

Costa, R. D. D., & Maciel, W. J. 1999, Ap&SS, 265, 327

Cuisinier, F., Acker, A., & Köppen, J. 1996, A&A, 307, 215

Cuisinier, F., Maciel, W. J., Köppen, J., Acker, A., & Stenholm, B. 2000, A&A, 353, 543

Escudero, A. V., & Costa, R. D. D. 2001, A&A, 380, 300

Fitzpatrick, E. L. 1999, PASP, 111, 63

Freitas Pacheco, J. A., Barbuy, B., Costa, R. D. D., & Idiart, T. 1993, A&A, 271, 429

Gathier, R., Pottasch, S. R., Goss, W. W., & van Gorkom, J. H. 1983, A&A, 128, 325

Kingdon, J., & Ferland, G. J. 1995, ApJ, 442, 714

Kingsburgh, R. L., & Barlow, M. J. 1994, MNRAS, 271, 257

Kohoutek, L. 1994, Ast. Nach., 315, 235

Köppen, J., Acker, A., & Stenholm, B. 1991, A&A, 248, 197

Liu, X.-W., Luo, S.-G., Barlow, M. J., Danziger, I. J., & Storey, P. J. 2001, MNRAS, 327, 141

Maciel, W. J. 1999, A&A, 351, 249

Maciel, W. J., Costa, R. D. D., & Uchida, M. M. M. 2003, A&A, 397, 667

Marigo, P. 2001, A&A, 370, 194

Mathis, J. S., Torres-Peimbert, S., & Peimbert, M. 1998, ApJ, 495, 328

Peimbert, M., & Torres-Peimbert, S. 1977, MNRAS, 179, 217

Péquignot, D., Petitjean, P., & Boisson, C. 1991, A&A, 251, 680

Pottasch, S. R. 1990, A&A, 236, 231

Ratag, M. A., Pottasch, S. R., Dennefeld, M., & Menzies, J. 1997, A&A, 126, 297

Rich, R. M. 1988, AJ, 95, 828

Rubin, R. H. 1986, ApJ, 309, 334

Samland, M., Köppen, J., Acker, A., & Stenholm, B. 1992, A&A, 264, 184

Schneider, S. E., & Buckley, D. 1996, ApJ, 459, 606

Stasińska, G., Tylenda, R., Acker, A., & Stenholm, B. 1992, A&A, 266, 486

Stasińska, G., Richer, M. G., & Mc Call, M. L. 1998, A&A, 336, 667

Torres-Peimbert, S., & Peimbert, M. 1977, Rev. Mex. Astron. Astrofis., 2, 181

van de Hoek, L. B., & Groenewegen, M. A. T. 1997, A&AS, 123, 305

van de Steene, G. C., & Zijlstra, A. A. 1995, A&A, 293, 541

Viegas, S. M., & Clegg, R. E. S. 1994, MNRAS, 271, 993

Zhang, C. Y. 1995, ApJS, 98, 659

Webster, L. 1988, MNRAS, 230, 377

Online Material

Table 2. Lines.

Line	Al 2-O	Bl 3-13	H 1-11	H 1-13	H 1-14	H 1-30	H 1-34	H 1-41	H 1-42	H 1-43	H 1-45
[OII]λ3727.7	52.8	–	3.0	–	14.9	35.1	17.3	22.8	10.4	–	–
[NeIII]λ3868.7	42.8	17.8	34.9	10.7	36.4	53.1	–	44.6	53.4	-	36.8
H6λ3889	10.5	5.4	9.4	–	6.9	–	5.5	9.3	8.8	6.18	5.4
[NeIII]λ3967.4	12.4	9.5	15.8	6.4	9.4	–	4.9	18.1	23.5	9.14	13.1
H5λ3970.1	–	–	1.4	–	3.3	21.6	–	–	–	–	–
H$\delta$$\lambda$4101.7	17.8	8.6	15.2	4.1	12.5	13.2	8.8	20.8	17.8	17.98	9.7
H$\gamma$$\lambda$4340.5	28.4	28.4	28.3	10.9	26.2	27.0	21.3	36.6	35.8	34.1	24.9
[OIII]λ4363.2	13.0	1.6	3.2	1.5	17.1	5.0	0.4	4.1	5.0	–	36.2
HeIλ4471.5	–	4.8	3.5	0.9	2.8	4.2	3.1	4.8	4.6	–	4.3
HeIIλ4685.7	58.0	–	3.3	6.8	18.9	19.8	–	21.4	1.0	–	28.2
[ArIV]λ4711.2	12.2	–	2.4	1.8	5.2	4.6	–	2.3	1.7	–	–
[ArIV]λ4740.2	8.8	–	1.7	3.7	3.4	4.5	–	1.6	1.6	–	3.8
H$\beta$$\lambda$4861.3	100.0	100.0	100.0	100.0	100.0	100.0	100.0	100.0	100.0	100.0	100.0
[OIII]λ4959.5	406.9	327.5	340.6	488.9	506.4	390.3	56.7	292.0	403.0	-	309.8
[OIII]λ5007.6	1336.1	1071.3	1065.4	1618.8	1614.9	1197.3	195.8	891.6	1242.5	2.52	1003.8
[NI]λ5199.1	–	–	–	–	–	5.0	–	–	–	1.1	-
[CaV]λ5309.2	–	–	–	–	–	–	–	–	–	–	4.8
HeIIλ5411.5	–	–	–	–	4.3	3.0	–	2.0	–	–	6.5
[CLIII]λ5517.7	–	–	–	–	–	1.4	–	0.6	0.5	–	–
[CLIII]λ5537.9	–	–	–	–	–	2.6	–	0.7	0.8	–	–
[NII]λ5754.6	8.1	–	–	4.7	1.0	12.9	3.0	0.4	0.5	0.86	2.7
HeIλ5875.8	36.5	38.4	30.1	99.5	30.1	37.9	5.1	20.5	25.2	2.93	71.8
[OI]λ6300.3	38.1	–	0.4	16.2	5.7	39.4	8.5	1.7	3.1	2.76	7.2
[SIII]λ6312.1	11.7	3.6	1.9	15.9	6.7	–	10.0	1.4	1.8	–	6.0
[OI]λ6363.8	12.6	–	–	5.9	1.9	11.9	3.0	0.5	1.0	1.04	1.8
[ArV]λ6434.7	7.4	–	–	–	–	1.5	–	–	–	–	4.1
[NII]λ6548.1	442.0	10.8	6.4	218.0	23.7	455.2	–	11.3	12.4	134.26	–
H$\alpha$$\lambda$6562.9	1203.5	1126.7	823.0	3922.8	1128.0	788.3	1176.6	420.2	563.8	619.36	1537.3
[NII]λ6583.5	1349.2	22.2	13.9	656.1	47.8	1451.4	787.8	23.6	23.4	423.72	19.2
HeIλ6678.2	22.5	16.8	12.7	67.8	13.0	15.4	16.4	6.3	8.4	2.62	28.5
[SII]λ6716.5	115.4	2.6	1.2	43.8	14.2	55.2	7.9	4.2	3.0	10.98	–
[SII]λ6730.9	107.0	3.7	1.7	73.3	16.6	104.7	13.0	6.7	4.5	21.73	–
[ArV]λ7005.6	23.7	–	–	–	3.4	4.7	–	–	–	0.81	14.9
HeIλ7065.5	20.6	20.8	14.2	142.8	20.0	23.5	20.1	4.3	14.5	1.86	125.7
[ArIII]λ7135.8	180.7	80.8	44.7	528.7	37.4	136.4	23.9	15.9	23.4	–	24.1
[ArIV]λ7170.5	–	–	–	–	3.5	–	-	–	–	–	13.2
HeIIλ7177.5	–	–	–	–	–	–	–	–	–	–	11.4
[ArIV]λ7238.1	–	2.1	1.8	13.2	1.7	1.3	–	–	–	2.79	7.2
[ArIV]λ7263	–	2.1	–	–	–	–	–	–	–	–	6.4
[OII]λ7319.4	26.7	4.3	1.6	57.6	6.8	22.7	16.5	4.5	9.5	3.24	18.1
[OII]λ7329.9	30.3	4.8	4.8	60.5	11.8	21.8	18.2	–	–	–	17.0
[ArIII]λ7751.4	42.9	20.2	14.5	195.5	15.7	–	3.6	–	–	–	

Table 2. continued.

Line	H 1-46	H 1-51	H 1-63	H 1-67	H 2-11	H 2-25	H 2-48	He 2-260	He 2-262	K 6-3	K 6-5
[OII]λ3727.7	24.3	1051.6	29.9	38.6	–	31.7	71.1	80.8	–	–	–
[NeIII]λ3868.7	11.9	131.2	11.0	54.7	–	–	–	–	9.4	–	–
H6λ3889	4.9	25.0	9.2	5.7	–	–	9.4	4.6	–	7.3	–
[NeIII]λ3967.4	11.1	52.1	8.9	–	–	3.6	–	–	8.1	–	–
H5λ3970.1	–	–	2.3	26.7	–	–	11.9	9.2	–	–	–
H$\delta\lambda$4101.7	13.5	31.2	19.7	19.2	–	9.5	18.9	19.4	7.8	-	-
H$\gamma\lambda$4340.5	30.7	62.3	41.3	36.6	18.0	24.7	38.0	37.8	25.2	16.4	-
[OIII]λ4363.2	2.0	8.7	3.1	6.4	1.2	–	0.6	–	–	1.6	–
HeIλ4471.5	4.0	11.5	4.3	2.9	–	–	2.4	–	3.7	–	–
HeIIλ4685.7	–	12.0	–	50.6	–	–	–	–	1.1	–	39.8
[ArIV]λ4711.2	–	–	0.8	6.3	–	–	–	1.0	–	–	–
[ArIV]λ4740.2	–	–	–	3.9	–	–	–	0.5	–	–	–
H$\beta\lambda$4861.3	100.0	100.0	100.0	100.0	100.0	100.0	100.0	100.0	100.0	100.0	100.0
[OIII]λ4959.5	180.0	247.3	139.0	376.5	153.6	24.6	36.2	1.6	289.0	127.5	250.1
[OIII]λ5007.6	571.6	546.3	430.6	1159.0	491.1	75.5	113.0	5.1	922.3	419.2	873.1
[NI]λ5199.1	0.3	13.6	-	1.7	–	–	–	–	–	–	–
[CaV]λ5309.2	–	–	–	–	–	–	–	–	–	–	–
HeIIλ5411.5	–	–	–	6.1	–	–	–	–	–	–	–
[CLIII]λ5517.7	0.5	–	–	1.3	–	–	0.3	–	–	–	–
[CLIII]λ5537.9	0.8	–	–	1.3	–	–	0.4	–	–	–	–
[NII]λ5754.6	3.3	5.9	4.1	2.3	14.2	2.6	5.6	4.1	–	5.7	35.6
HeIλ5875.8	32.6	20.7	20.5	17.7	106.7	37.4	13.6	2.1	63.4	112.5	107.0
[OI]λ6300.3	4.9	60.8	2.5	6.5	18.8	3.6	4.7	3.5	10.0	36.5	213.4
[SIII]λ6312.1	4.0	-	3.9	6.1	8.8	4.8	2.4	1.3	6.3	12.8	51.4
[OI]λ6363.8	1.7	26.9	0.9	2.8	5.6	-	1.7	1.1	3.1	12.3	53.6
[ArV]λ6434.7	–	–	–	–	–	–	–	–	–	–	–
[NII]λ6548.1	44.0	189.3	20.4	65.9	699.1	167.3	53.6	59.6	69.2	752.3	2218.9
H$\alpha\lambda$6562.9	774.9	609.7	448.2	546.6	2862.9	1649.2	586.1	498.9	1955.8	4105.9	5071.1
[NII]λ6583.5	127.6	990.3	61.3	187.9	2236.4	528.5	196.6	183.8	198.6	2355.1	7013.3
HeIλ6678.2	11.9	11.3	5.6	7.0	61.8	18.7	4.1	0.5	29.7	98.2	71.6
[SII]λ6716.5	3.4	244.5	0.7	22.0	25.0	20.8	2.3	4.2	15.6	160.5	674.5
[SII]λ6730.9	6.1	202.9	1.5	29.4	57.8	20.6	4.6	9.0	26.7	228.5	850.3
[ArV]λ7005.6	–	–	–	–	–	–	0.3	0.9	–	–	77.9
HeIλ7065.5	30.2	10.1	15.7	6.2	155.0	27.4	9.4	1.1	52.6	102.6	97.2
[ArIII]λ7135.8	34.7	46.4	20.0	51.5	410.8	53.6	9.0	1.6	135.9	277.9	1324.6
[ArIV]λ7170.5	–	–	–	–	–	–	–	–	–	–	–
HeIIλ7177.5	–	–	–	–	–	–	–	–	–	–	–
[ArIV]λ7238.1	–	–	–	–	13.3	–	–	–	–	56.0	–
[ArIV]λ7263	–	–	–	–	15.1	–	0.8	–	–	–	256.8
[OII]λ7319.4	42.2	19.4	44.6	10.4	108.7	50.8	113.2	35.8	37.1	104.0	73.0
[OII]λ7329.9	40.5	12.1	48.6	–	62.2	45.9	–	41.2	35.5	–	65.1
[ArIII]λ7751.4	–	–	–	–	–	12.3	–	–	50.1	92.0	176.4

Table 2. continued.

Line	KFL 2	KFL 4	KFL 19	M 1-31	M 1-48	M 2-7	M 2-8	M 2-12	M 2-13	M 2-15	M 2-20
[OII]λ3727.7	–	–	12.0	12.9	111.8	80.7	29.7	31.7	69.4	10.4	–
[NeIII]λ3868.7	43.1	23.7	27.1	19.9	48.9	6.4	39.4	–	45.2	43.1	–
H6λ3889	10.4	–	7.7	4.8	11.2	11.4	9.2	5.5	11.2	11.5	4.0
[NeIII]λ3967.4	15.8	6.2	5.8	7.1	19.2	7.9	20.6	–	13.1	20.3	2.8
H5λ3970.1	18.0	–	–	–	–	1.8	–	7.8	3.5	1.2	–
H$\delta$$\lambda$4101.7	23.3	13.4	10.5	10.8	18.7	19.1	12.8	17.4	18.0	20.1	3.4
H$\gamma$$\lambda$4340.5	40.5	16.8	25.5	26.7	37.0	37.9	34.9	36.0	35.8	34.9	25.6
[OIII]λ4363.2	18.4	11.6	3.1	1.0	1.9	–	4.6	0.4	3.0	2.9	1.4
HeIλ4471.5	5.4	–	3.3	4.9	5.6	4.8	6.2	–	4.8	4.7	5.6
HeIIλ4685.7	64.3	32.5	–	–	10.6	–	26.9	–	–	22.7	5.4
[ArIV]λ4711.2	10.4	6.4	–	–	–	–	–	–	1.0	2.9	–
[ArIV]λ4740.2	11.2	5.2	–	–	0.8	–	3.9	–	0.4	1.9	–
H$\beta$$\lambda$4861.3	100.0	100.0	100.0	100.0	100.0	100.0	100.0	100.0	100.0	100.0	100.0
[OIII]λ4959.5	324.6	400.7	255.4	289.5	232.0	74.2	311.3	-	300.0	270.0	216.1
[OIII]λ5007.6	963.5	1175.0	789.0	918.0	705.2	234.4	936.1	0.9	928.2	835.6	724.2
[NI]λ5199.1	–	–	–	1.3	7.7	1.0	2.3	1.1	2.9	–	–
[CaV]λ5309.2	–	–	–	–	–	–	–	–	–	–	–
HeIIλ5411.5	15.2	–	–	–	1.4	–	3.6	–	–	2.6	–
[CLIII]λ5517.7	–	–	–	0.8	1.4	0.6	1.3	–	0.7	0.7	–
[CLIII]λ5537.9	–	–	–	1.8	1.4	–	1.9	–	1.0	0.7	–
[NII]λ5754.6	–	–	–	7.2	7.7	1.1	4.3	2.1	4.5	1.0	2.0
HeIλ5875.8	14.4	22.1	13.2	62.7	30.9	34.0	50.9	2.8	29.4	29.7	28.4
[OI]λ6300.3	–	–	1.4	21.7	33.1	4.1	19.4	2.9	17.2	0.4	5.2
[SIII]λ6312.1	–	-	1.2	6.6	3.1	0.6	–	–	3.6	1.7	4.6
[OI]λ6363.8	–	–	–	7.4	10.7	1.6	5.4	–	5.7	–	1.3
[ArV]λ6434.7	–	–	–	–	–	–	–	–	–	–	–
[NII]λ6548.1	–	–	1.3	185.2	314.2	73.2	110.2	137.1	110.8	12.7	128.4
H$\alpha$$\lambda$6562.9	504.9	773.0	335.2	1170.1	571.3	623.1	673.9	661.0	617.1	649.8	1163.0
[NII]λ6583.5	11.4	3.7	4.3	572.4	1001.3	218.4	420.4	416.2	345.5	36.2	429.2
HeIλ6678.2	7.3	10.5	3.8	24.5	10.9	9.6	13.0	0.9	10.4	11.2	18.2
[SII]λ6716.5	–	–	1.6	14.1	71.5	24.7	24.3	22.2	16.7	4.0	16.2
[SII]λ6730.9	–	–	0.6	23.7	97.5	27.3	33.7	43.1	29.0	5.9	19.8
[ArV]λ7005.6	–	–	–	–	–	–	–	–	–	–	–
HeIλ7065.5	–	10.5	3.6	56.6	9.6	6.0	16.5	0.8	16.1	8.3	15.4
[ArIII]λ7135.8	20.0	18.8	8.0	152.9	58.1	26.3	51.2	2.2	41.7	38.5	51.4
[ArIV]λ7170.5	–	–	–	–	–	–	–	–	–	–	–
HeIIλ7177.5	–	–	–	–	–	–	–	–	–	–	–
[ArIV]λ7238.1	–	–	–	2.6	1.1	2.1	2.8	1.2	–	5.6	3.0
[ArIV]λ7263	–	9.9	–	5.6	–	–	–	–	–	–	–
[OII]λ7319.4	–	–	–	37.4	18.4	3.3	20.5	5.0	17.3	5.9	17.6
[OII]λ7329.9	–	–	–	34.7	–	4.3	–	5.1	18.4	6.5	15.9
[ArIII]λ7751.4	–	–	2.3	48.7	–	6.6	13.7	–	13.2	10.5	26.7

Table 2. continued.

Line	M 2-26	M 2-38	M 2-39	M 3-9	M 3-19	M 3-26	M 3-32	M 3-33	M 3-37	M 3-52	M 3-54
[OII]λ3727.7	16.0	32.3	24.2	–	–	14.2	16.1	6.2	151.4	–	–
[NeIII]λ3868.7	13.3	63.0	29.8	34.0	23.9	60.0	44.0	65.2	48.5	–	45.1
H6λ3889	3.0	12.1	7.2	5.1	8.8	13.7	14.8	11.1	9.4	–	5.6
[NeIII]λ3967.4	9.6	26.3	–	11.3	–	21.0	–	–	20.8	–	0.8
H5λ3970.1	–	–	15.5	–	17.7	–	23.6	28.3	–	–	17.4
H$\delta$$\lambda$4101.7	12.7	27.6	17.4	10.4	21.0	24.4	24.0	18.3	13.3	–	15.2
H$\gamma$$\lambda$4340.5	33.6	47.8	36.3	11.2	40.4	39.0	40.9	32.5	31.3	–	29.5
[OIII]λ4363.2	2.5	9.2	18.8	3.7	4.2	3.2	3.0	7.6	3.7	–	5.9
HeIλ4471.5	5.8	5.0	5.0	-	10.3	5.7	5.7	4.1	4.4	–	2.8
HeIIλ4685.7	17.3	100.5	0.8	23.6	4.2	31.4	11.7	21.5	10.2	10.6	42.5
[ArIV]λ4711.2	–	14.1	–	2.9	–	3.2	2.3	4.0	–	–	5.7
[ArIV]λ4740.2	–	11.4	–	1.0	–	1.9	1.5	3.3	–	–	4.8
H$\beta$$\lambda$4861.3	100.0	100.0	100.0	100.0	100.0	100.0	100.0	100.0	100.0	100.0	100.0
[OIII]λ4959.5	218.6	301.8	138.1	319.4	149.6	202.8	234.3	378.3	362.4	254.9	392.6
[OIII]λ5007.6	689.0	820.1	429.3	998.9	446.5	598.6	754.6	1105.7	1133.3	810.1	1212.3
[NI]λ5199.1	3.5	1.8	–	–	–	–	–	–	9.1	–	–
[CaV]λ5309.2	–	–	–	–	–	–	–	–	–	–	–
HeIIλ5411.5	3.1	8.9	–	3.4	–	3.1	1.4	1.8	–	–	5.8
[CLIII]λ5517.7	–	1.5	–	–	–	–	0.6	–	–	–	0.9
[CLIII]λ5537.9	–	1.8	–	–	–	–	0.7	–	–	–	0.9
[NII]λ5754.6	4.4	1.6	1.1	–	–	1.6	0.8	–	12.2	15.9	–
HeIλ5875.8	42.6	10.4	26.7	12.8	22.1	27.5	24.8	9.6	28.6	48.5	24.2
[OI]λ6300.3	9.6	3.7	5.1	6.9	–	0.4	0.3	0.4	87.7	98.9	–
[SIII]λ6312.1	4.2	5.3	2.6	–	–	1.3	1.4	0.8	4.8	9.6	2.1
[OI]λ6363.8	3.6	1.7	1.9	2.1	–	–	–	–	30.1	34.4	–
[ArV]λ6434.7	–	2.4	–	–	–	5.7	–	–	–	–	–
[NII]λ6548.1	245.0	17.3	30.4	7.5	18.8	10.0	11.7	1.3	481.9	866.2	–
H$\alpha$$\lambda$6562.9	835.8	307.7	622.5	1101.5	484.2	454.2	448.9	402.7	1094.2	1420.7	851.8
[NII]λ6583.5	771.5	41.3	71.4	25.7	47.9	26.1	34.4	3.2	1507.4	2464.6	8.4
HeIλ6678.2	19.1	7.3	9.4	17.3	21.6	10.0	8.4	4.8	16.1	33.1	10.8
[SII]λ6716.5	67.8	10.7	4.7	4.1	–	3.1	4.2	0.4	100.5	398.6	1.6
[SII]λ6730.9	59.3	12.0	7.3	5.9	–	3.8	6.0	0.6	112.0	359.0	2.1
[ArV]λ7005.6	–	5.2	–	–	–	–	–	–	–	–	–
HeIλ7065.5	11.9	4.9	19.5	10.2	18.5	5.3	6.0	3.9	18.9	–	7.3
[ArIII]λ7135.8	98.2	32.2	21.2	59.6	37.8	26.8	24.4	10.9	114.5	211.7	42.3
[ArIV]λ7170.5	–	–	–	–	–	–	–	–	–	–	–
HeIIλ7177.5	–	3.2	–	–	–	–	–	0.3	–	–	–
[ArIV]λ7238.1	8.9	–	0.8	5.9	12.1	6.2	3.5	0.3	–	–	–
[ArIV]λ7263	–	–	–	4.5	–	–	–	–	–	–	–
[OII]λ7319.4	11.9	4.8	6.0	10.9	12.1	6.3	4.1	1.5	34.9	92.3	6.3
[OII]λ7329.9	11.8	3.0	5.7	4.5	17.9	2.5	4.0	1.2	26.1	-	5.3
[ArIII]λ7751.4	19.8	–	–	–	12.0	6.5	7.2	3.0	28.3	-	-

Table 2. continued.

Line	M 4-4	M 4-6	M 4-7	M 4-8	Pe 1-12	Pe 1-13	Th 3-13	Th 3-15	Th 3-34	Th 4-2	Th 4-7
[OII]λ3727.7	–	–	–	34.2	–	–	–	25.4	–	40.2	–
[NeIII]λ3868.7	–	24.2	30.6	–	38.4	59.3	–	–	–	33.9	45.5
H6λ3889	–	3.5	23.3	–	10.1	–	–	–	–	6.6	22.8
[NeIII]λ3967.4	–	10.1	11.4	–	9.1	23.7	–	–	–	10.6	20.9
H5λ3970.1	–	–	–	–	7.0	–	–	–	–	3.2	–
H$\delta\lambda$4101.7	13.0	5.9	7.9	8.9	19.2	23.9	–	12.1	–	17.9	10.3
H$\gamma\lambda$4340.5	27.1	18.0	18.3	22.6	37.1	40.5	15.6	27.4	15.8	31.5	26.1
[OIII]λ4363.2	–	5.1	10.7	–	8.0	14.9	–	3.1	12.3	3.3	16.3
HeIλ4471.5	–	–	–	–	–	–	–	3.8	–	5.3	3.3
HeIIλ4685.7	43.9	10.4	8.9	–	103.6	97.8	–	–	55.7	31.9	–
[ArIV]λ4711.2	–	2.8	–	–	7.7	12.6	–	–	–	–	–
[ArIV]λ4740.2	–	5.3	–	–	5.7	11.6	–	–	16.0	–	–
H$\beta\lambda$4861.3	100.0	100.0	100.0	100.0	100.0	100.0	100.0	100.0	100.0	100.0	100.0
[OIII]λ4959.5	363.1	633.9	531.8	2.6	194.4	300.3	274.7	176.6	508.1	208.3	532.6
[OIII]λ5007.6	1232.5	2046.2	1723.7	8.1	588.7	875.4	902.5	558.9	1851.1	649.8	1685.3
[NI]λ5199.1	6.8	–	–	–	–	–	–	–	–	4.2	–
[CaV]λ5309.2	–	–	–	–	–	–	–	–	–	–	–
HeIIλ5411.5	–	–	–	–	6.5	8.9	–	–	35.2	3.5	9.7
[CLIII]λ5517.7	–	–	–	–	–	–	–	–	–	–	–
[CLIII]λ5537.9	–	–	–	–	–	–	–	–	–	–	–
[NII]λ5754.6	6.1	7.4	2.9	7.0	1.0	–	13.2	–	152.7	5.2	2.9
HeIλ5875.8	57.2	81.9	51.0	7.6	4.9	2.1	98.6	36.5	266.3	32.5	23.3
[OI]λ6300.3	23.8	60.9	25.7	6.8	–	1.2	29.0	26.2	152.0	14.8	41.8
[SIII]λ6312.1	14.8	17.4	10.0	3.7	–	2.1	33.9	1.8	243.1	3.5	8.5
[OI]λ6363.8	9.2	23.3	–	3.0	–	–	13.8	9.6	49.8	4.7	13.7
[ArV]λ6434.7	–	–	–	–	–	1.9	–	–	182.7	–	–
[NII]λ6548.1	367.5	199.9	76.5	204.9	–	–	179.6	74.2	2403.2	211.1	73.3
H$\alpha\lambda$6562.9	2028.0	3208.9	2092.0	1718.6	368.6	474.9	3534.5	1122.5	7821.6	526.2	929.3
[NII]λ6583.5	1086.1	625.7	227.9	684.2	3.5	2.8	555.8	189.9	7443.5	648.5	195.6
HeIλ6678.2	33.2	50.6	28.9	2.3	3.9	2.2	57.6	15.2	256.0	13.7	8.7
[SII]λ6716.5	95.2	46.1	36.4	19.6	0.8	–	16.4	59.6	143.5	79.0	21.6
[SII]λ6730.9	111.1	85.5	50.3	37.7	1.5	–	25.2	60.8	262.5	72.5	31.7
[ArV]λ7005.6	–	14.4	–	–	–	5.0	–	–	753.5	–	6.1
HeIλ7065.5	28.5	128.4	44.5	7.1	–	–	209.9	11.8	945.1	6.3	17.2
[ArIII]λ7135.8	259.2	322.6	98.5	7.2	9.4	13.6	577.4	42.7	2609.3	64.7	48.0
[ArIV]λ7170.5	–	–	–	–	–	–	–	–	218.7	–	3.3
HeIIλ7177.5	–	–	–	–	1.6	–	–	–	–	–	–
[ArIV]λ7238.1	–	–	–	–	–	–	–	–	125.3	–	4.0
[ArIV]λ7263	–	–	–	–	–	–	–	–	106.0	–	–
[OII]λ7319.4	27.9	121.5	42.0	164.7	2.0	–	345.8	65.4	431.6	6.3	38.8
[OII]λ7329.9	27.2	132.6	38.7	129.7	1.1	–	316.7	–	444.1	1.0	36.5
[ArIII]λ7751.4	74.4	106.8	19.8	–	–	–	203.1	–	1796.0	7.0	21.8

Table 2. continued.

Line	Vy 2-1	Y-C 2-32
[OII]λ3727.7	58.0	9.2
[NeIII]λ3868.7	32.0	45.3
H6λ3889	17.3	13.2
[NeIII]λ3967.4	–	23.0
H5λ3970.1	20.7	–
H$\delta\lambda$4101.7	25.5	19.9
H$\gamma\lambda$4340.5	46.0	29.5
[OIII]λ4363.2	1.2	3.7
HeIλ4471.5	6.7	4.9
HeIIλ4685.7	0.7	3.5
[ArIV]λ4711.2	–	2.4
[ArIV]λ4740.2	–	1.5
H$\beta\lambda$4861.3	100.0	100.0
[OIII]λ4959.5	218.0	273.1
[OIII]λ5007.6	637.1	807.1
[NI]λ5199.1	0.8	–
[CaV]λ5309.2	–	–
HeIIλ5411.5	–	–
[CLIII]λ5517.7	0.8	–
[CLIII]λ5537.9	0.9	–
[NII]λ5754.6	2.1	–
HeIλ5875.8	20.3	15.1
[OI]λ6300.3	8.3	0.3
[SIII]λ6312.1	–	0.7
[OI]λ6363.8	2.2	–
[ArV]λ6434.7	–	–
[NII]λ6548.1	102.7	2.4
H$\alpha\lambda$6562.9	280.9	378.0
[NII]λ6583.5	150.4	5.6
HeIλ6678.2	8.7	5.6
[SII]λ6716.5	13.4	0.5
[SII]λ6730.9	14.7	0.8
[ArV]λ7005.6	–	–
HeIλ7065.5	11.1	4.6
[ArIII]λ7135.8	26.9	14.2
[ArIV]λ7170.5	–	–
HeIIλ7177.5	–	–
[ArIV]λ7238.1	–	0.6
[ArIV]λ7263	–	–
[OII]λ7319.4	16.9	1.7
[OII]λ7329.9	–	1.5
[ArIII]λ7751.4	9.4	–